SAND2016-5314 J

PFLOTRAN-E4D: A parallel open source PFLOTRAN module for simulating time-lapse electrical resistivity data

Timothy C. Johnson[1*], Glenn E. Hammond[2], and Xingyuan Chen[1]

[1] Pacific Northwest National Laboratory
902 Battelle Boulevard
P.O. Box 999, MSIN K9-33
Richland, WA 99352 USA
email: tj@pnnl.gov

[2] Sandia National Laboratory
P.O. Box 5800 MS 0747
Albuquerque, NM 87185-0747 USA
Email: gehammo@sandia.gov

* Corresponding author

1. Abstract

Time-lapse electrical resistivity tomography (ERT) is finding increased application for remotely monitoring processes occurring in the near subsurface in three-dimensions (i.e. 4D monitoring). However, there are few codes capable of simulating the evolution of subsurface resistivity and corresponding tomographic measurements arising from a particular process, particularly in parallel and with an open source license. Herein we describe and demonstrate an electrical resistivity tomography module for the PFLOTRAN subsurface simulation code, named PFLOTRAN-E4D. The PFLOTRAN-E4D module operates in parallel using a dedicated set of compute cores in a master-slave configuration. At each time step, the master processes receives subsurface states from PFLOTRAN, converts those states to bulk electrical conductivity, and instructs the slave processes to simulate a tomographic data set. The resulting multi-physics simulation capability enables accurate feasibility studies for ERT imaging, the identification of the ERT signatures that are unique to a given process, and facilitates the joint inversion of ERT data with hydrogeological data for subsurface characterization. PFLOTRAN-E4D is demonstrated herein using a field study of stage-driven groundwater/river water interaction ERT monitoring along the Columbia River, Washington, USA. Results demonstrate the complex nature of subsurface electrical conductivity changes, in both the saturated and unsaturated zones, arising from water table fluctuation and from river water intrusion into the aquifer. The results also demonstrate the sensitivity of surface based ERT measurements to those changes over time. PFLOTRAN-E4D is available with the PFLOTRAN development version with an open-source license at https://bitbucket.org/pflotran/pflotran-dev .

2. Key Words

resistivity, groundwater, simulation, multi-physics, parallel, open-source, forward modeling

3. Introduction

Electrical Resistivity Tomography (ERT) is a geophysical imaging application whereby the bulk electrical conductivity (i.e. the reciprocal of resistivity) distribution of the subsurface is remotely estimated. ERT has found wide application for understanding the near subsurface because bulk conductivity is governed by both the structural and geochemical properties that determine subsurface interactions [*Revil et al.*, 2012]. More recently, time-lapse ERT developments have enabled subsurface processes to be monitored in terms of spatial and temporal changes in bulk conductivity [*Binley et al.*, 2015; *Kemna et al.*, 2006; *Singha et al.*, 2015]. Time-lapse imaging allows the static contributions of bulk conductivity to be removed, thereby revealing the temporal evolution of spatial changes in bulk conductivity. These changes can often be uniquely related to some subsurface process (e.g. fluid transport, geochemical alteration etc.), thereby providing the capability to remotely monitor that process in space and time (see previous references for examples).

Despite the growing popularity of time-lapse ERT imaging, multi-physical simulation codes designed specifically to simulate changes in subsurface bulk conductivity arising from some subsurface process, and then to simulate the corresponding time-lapse ERT data arising from that process, are lacking. Because of this, ERT practitioners have limited tools for investigating the feasibility or performance of a time-lapse ERT imaging campaign for a particular subsurface process prior to field trial. The resulting uncertainty raises the risk of failure and reduces the overall utility of ERT imaging. In addition, ERT survey design, which comprises both electrode layout and measurement sequence, is typically based on standardized applications, as opposed to being customized to a particular anticipated subsurface process. The capability to accurately simulate the ERT data arising from that process given multiple survey design scenarios would facilitate customized survey designs to improve imaging resolution in both space and time. It would also enable the discovery of critical electrical signatures associated with some processes of interest, and the exploitation of that signature for effective process monitoring. Such a simulator would also facilitate the use of time lapse ERT data in hydrogeological parameter estimation (deterministic and stochastic) algorithms [*Commer et al.*, 2014; *Linde et al.*, 2006; *Rings et al.*, 2010]. Given the recent advancements in understanding the mechanistic relationships between bulk conductivity and subsurface structural and geochemical states [*Revil*, 2013; *Slater*, 2007 and references therein], the capability to accurately derive bulk conductivity from existing subsurface simulators is within reach.

In this work we describe a parallel ERT computing module for PFLOTRAN [*Hammond et al.*, 2014], a massively parallel reactive flow and transport model for simulating surface and subsurface processes. Using Message Passing Interface (MPI) libraries [*Gropp et al.*, 1999], a group of processors is created exclusively to accommodate ERT forward modeling. After each time step, PFLOTRAN passes relevant simulation results to this group of modules, which are then transformed to subsurface bulk conductivity, and used to compute a simulated ERT survey for that time step. We demonstrate the code using a groundwater/surface water interaction simulation based upon actual field data. The results show the complex nature of the changes in bulk conductivity arising from stage-driven changes in water table elevation and groundwater/surface water interaction. The results also demonstrate the sensitivity of the ERT data to these processes, thereby validating the capability to monitor them at the field scale. The code and user documentation are available with the PFLOTRAN distribution and associated open source license (https://bitbucket.org/pflotran/pflotran-dev).

4. Methods

4.1. E4D (background, capabilities, parallel structure)

E4D is a parallel ERT forward modeling and inversion code available with a Berkeley Software Distribution open source license [*T.C. Johnson and Wellman*, 2015a; *T. C. Johnson et al.*, 2010] (see (https://e4d.pnnl.gov). The ERT method uses hardware and software to image the bulk electrical conductivity of the subsurface. Bulk electrical conductivity is influenced by physical, biological, and geochemical interactions, making time-lapse images of changes in bulk conductivity useful for monitoring subsurface processes. Measurements are collected using a four-electrode configuration, whereby current is injected between a source and a sink electrode, and the resulting electrical potential is measured between a positive and negative potential electrode. The ratio of the observed potential to the current injected (or some transform thereof) is called the transfer resistance, and constitutes the primary ERT measurement [*Daily and Owen*, 1991]. In a typical ERT survey, hundreds to tens of thousands of such measurements are strategically collected using array of static electrodes deployed along the surface and/or within boreholes. Time-lapse data sets consist of many identical ERT surveys collected over time to monitor the changes in transfer resistance associated with some subsurface process of interest. Forward modeling is the process whereby the transfer resistance measurements are simulated, given the subsurface bulk conductivity distribution in space and time.

ERT imaging involves inverting the transfer resistance measurements to estimate the bulk conductivity distribution that gave rise the measurements. In comparison to forward modeling, the inversion processes is computationally demanding in terms of both CPU load and memory requirements. Details concerning the parallel inversion may be found in Johnson et al., (2010). The work herein focuses on forward modeling, where the subsurface bulk conductivity distribution is generated by converting subsurface states simulated by PFLOTRAN to bulk conductivity using a petrophysical transform. The petrophysical transform is defined herein as the relationship between hydrogeological properties and states and the corresponding subsurface bulk conductivity.

The direct-current electrical potential arising from a given current source is given by the Poisson equation

$$\nabla \cdot \sigma_b(\mathbf{r}) \nabla \phi(\mathbf{r}) = -\nabla \cdot J(\mathbf{r})$$

eq. 1

where $\mathbf{r}$ is a position vector, σ_b is effective bulk electrical conductivity, ϕ is electrical potential, and J is the source current density. Given σ, J, and appropriate boundary conditions, the objective of the forward model is to solve eq. **Error! Reference source not found.** for ϕ, which is measured during an ERT experiment. Because potential is a linear function of current density, equation 1 can be solved by superimposing solutions with different current source terms. A pole solution is a solution to equation 1 for a given point source of current with a current sink at infinite distance from the source. Because there are typically many more current source injections than electrodes for a given ERT survey, it is generally more efficient to model the pole solutions for each electrode, and then subtract the pole solution for the sink electrode from the pole solution for the source electrode to simulate the potential field generated by a particular source sink pair. In this way, the number of solutions to equation 1 required to simulate an ERT survey is equal to the number of electrodes instead of the number of measurements.

We use the forward modeling capabilities of E4D to simulate time-lapse ERT surveys in this paper. E4D solves equation 1 using the finite element method on an unstructured tetrahedral mesh. Details concerning numerical aspects of the forward solution can be found in Rucker et al. (2006) and Johnson et al., (2010). Details concerning the parallelization are found in Johnson et al. (2010), and the forward computations are summarized by the flow diagram in Figure 1. Numerous aspects of Figure 1 are discussed in the forthcoming sections, including the PFLOTRAN-E4D coupling, mesh interpolation and petrophysical transformation. Of note here are the master-slave configuration of E4D and the highly parallel nature of the E4D forward computations. In particular, E4D has one master process that provides the communication link to PFLOTRAN and orchestrates all E4D computations. Slave nodes accommodate the primary computational burdens and memory requirements, and communicate only with the master node during pre and post solution phases through MPI broadcast calls, making the forward modeling highly scalable.

4.2. PFLOTRAN (background, capabilities, parallel structure)

PFLOTRAN is a massively-parallel multi-physics simulator [Hammond et al., 2014]. PFLOTRAN has simulated subsurface multiphase flow and reactive biogeochemical transport since its inception, and those process models continue to be enhanced. More recently, geomechanics, surface water flow (along with coupling to land surface models), and nuclear waste form process models have been added to the code. PFLOTRAN is written in object oriented FORTRAN 2003/2008 and founded upon the PETSc framework [Balay et al., 2015], which provides the underlying parallel data structures and solvers for scalable high performance computing. The code's parallelization is based on domain decomposition and the use of MPI libraries. Key FORTRAN 2003/2008 features leveraged by PFLOTRAN include the FORTRAN class (i.e. extensible, polymorphic derived types with member functions) and pointers to procedures which improve code reuse and minimize the use of conditionals and cumbersome select case statements throughout the code.

PFLOTRAN has been executed on problems composed of over 3 billion degrees of freedom and utilizing up to 262,144 processes, though the code is more commonly employed on problems with millions to tens of millions of degrees of freedom utilizing hundreds to thousands of processes. Note that although PFLOTRAN is designed for massively parallel computation, the same single code base can run on a single process without recompilation, though available memory may be a limitation. The code is developed primarily on laptops and desktops running a variety of operating systems (i.e. Linux, Mac OS, Windows) and the GNU and Intel compilers. PFLOTRAN is developed and distributed under an open source GNU LGPL license.

PFLOTRAN's object oriented design facilitates the incorporation of new process models within the code and/or coupling with code developed externally (e.g. E4D). This design is described in detail below. Lichtner et al. (2015) provides a comprehensive overview of PFLOTRAN capability.

For the demonstration in this paper, PFLOTRAN simulated single phase variably saturated flow and solute transport in the subsurface. Single-phase variably saturated flow is based on the Richards equation with the form

$$\frac{\partial}{\partial t}(\varphi s \rho) + \nabla \cdot \rho \boldsymbol{q} = 0,$$

eq. 2

with water density ρ, porosity φ, and saturation s. The Darcy velocity $\boldsymbol{q}$ is given by

$$\boldsymbol{q} = -\frac{k k_r}{\mu} \nabla (p - \rho g \boldsymbol{z}),$$

eq. 3

with water pressure p, viscosity μ, acceleration of gravity g, intrinsic permeability k, relative permeability k_r. Conservative solute transport in the liquid phase is based on the advection-dispersion equation

$$\frac{\partial}{\partial t}(\varphi s C) + \nabla \cdot (\boldsymbol{q} - \varphi s D \nabla) C = 0,$$

eq. 4

with solute concentration C and dispersion coefficient D. PFLOTRAN employs backward Euler time discretization and the Newton-Raphson method (where necessary) to solve for flow and transport state variables over time.

4.3. PFLOTRAN-E4D coupling

In 2014, PFLOTRAN's software architecture was refactored extensively to improve flexibility with regard to source code development. Through the use of FORTRAN 2003/2008 classes, the workflow of simulation execution was refactored into a tree structure of hierarchical process models (multiphysics processes coupled to numerical methods). As process models are added to PFLOTRAN, factories are adapted or created to accommodate these new process models classes. During simulation initialization, these factories set up process models and link them within a tree data structure (tree graph theory). Each process model has two pointers: one to a child and another to a peer process model as shown in Figure 2. If no child or peer process model exists, the pointers remain null.

Peer process models synchronize at specified times while descendants play catch up at their own pace (i.e. a descendant can sub-step to catch up to its parent). Therefore, for the process model tree shown in Figure 3, the master process model A executes first taking as many time steps as necessary to reach a synchronization point. For each A time step, B takes as many time steps as necessary to catch up to A (this may be a single time step [i.e. B is lock step with A] or multiple time steps). Once A (and it's child B) have reached the synchronization point, C time steps until it reaches the same point in time. Key state variables and parameters are updated between A and C at the synchronization point and between A and B before and after each of A's time steps.

For the PFLOTRAN-E4D coupling, the linkage is simple. Flow serves as the master process model with solute transport as its child, and geophysics is the descendant of solute transport as shown in Figure 4. After each transport step, solute concentrations and water saturations are passed to E4D. Note that E4D's execution is non-blocking. Once PFLOTRAN hands off the state variables (i.e. solute concentration and water saturation), the flow and transport process models can proceed with their execution before E4D has completed its step since E4D runs in a separate set of processes. However, the handoff of state variables after the subsequent transport step must wait until E4D has completed its step, if necessary.

4.4. Initialization

Inter-process communications in both PFLOTRAN and E4D are governed using direct MPI calls. MPI enables groups of processes to be organized into communicator groups, where each process in the group is able to communicate with any other process in the group. Each process may belong to one or more communicator groups. Upon initialization, PFLOTRAN divides the available compute cores between PFLOTRAN and E4D as directed by user input, and creates two additional communicator groups to accommodate the E4D simulation module. The first of these groups contains one PFLOTRAN process and the E4D master process, and provides the link by which information is passed from PFLOTRAN to E4D. The second communicator group contains the E4D master process and slave processes, which execute all E4D computations. Once the E4D module is initialized, both PFLOTRAN and E4D proceed to read their respective input files and execute pre-simulation setup. This includes generation of the PFlOTRAN-to-E4D mesh interpolation matrix generated by E4D as described in section 4.7. The mesh interpolation matrix is used to accurately transfer PFLOTRAN state simulations from the PFLOTRAN mesh to the E4D mesh.

4.5. PFLOTRAN->E4D data transfer

Once setup computations are complete, PFLOTRAN begins the subsurface simulation. Upon completion of each time step, PFLOTRAN passes relevant states (e.g. fluid conductivity, saturation, tracer concentration etc.) to the E4D master node and proceeds to the next time step. The E4D master node then determines whether an E4D simulation is required for the current time step, as specified by user input. If a forward simulation is required, the PFLOTRAN states are converted to bulk conductivity and mapped to the E4D mesh by the E4D master node as described in sections 4.6 and 4.7 (Figure 1B).

The master node then broadcasts the bulk conductivity distribution to the E4D slave nodes and instructs them to execute a forward run as described in section 4.8. If a forward run is not required for the current time step, E4D waits for the next time step. Thus, in terms of timing, E4D follows behind PFLOTRAN, executing a forward simulation for the current time step while PFLOTRAN proceeds to simulate the subsurface states for the next time step.

4.6. Petrophysical Transform

On its own, bulk electrical conductivity is generally not considered a property of primary importance for most subsurface applications, and is therefore not simulated by most subsurface simulators. However, bulk conductivity is governed by variables (i.e. subsurface properties and/or states) that are often considered primary, and are therefore directly simulated by subsurface simulation codes. The direct relationship between these primary variables and bulk conductivity enables spatial and temporal changes in bulk conductivity to be interpreted in terms of corresponding properties and processes. That relationship is termed herein the petrophysical transform, and provides the mathematical link for transforming relevant states simulated by PFLOTRAN to bulk electrical conductivity.

A detailed derivation of the petrophysical transform demonstrated in this work is provided by Revil (2013), and is given by

$$\sigma_b = \Phi^m \left[s_w^n \sigma_w + (\Phi^{-m} - 1)\sigma_s \right], \qquad \text{eq. 5}$$

where Φ is porosity, m is the cementation exponent [*Archie*, 1942] which accounts for the effects for tortuosity, s_w is fluid saturation, n is the saturation exponent, σ_w is the fluid conductivity, and σ_s is the surface conductivity. The surface conductivity term accounts for current conduction at the pore-grain interface. PFLOTRAN is capable of directly simulating the state of each parameter on the right hand side of equation 5, or computing the parameters necessary to derive those changes. Each of these parameters can either be passed to E4D by PFLOTRAN, or be specified as a static variable in the E4D input files, in order to compute the bulk conductivity distribution. PFLOTRAN is also capable of simulating temperature, which can be included as part of the petrophysical transform. Once the relevant parameters and state variables are passed to E4D by PFLOTRAN, the E4D master node uses equation 5 to determine bulk conductivity on the PFLOTRAN mesh, and then interpolates those results to the E4D mesh using the approach described in the next section.

4.7. Mesh interpolation matrix

Once simulated states are transferred from PFLOTRAN to E4D at a given time step, those states must be transformed to bulk conductivity and mapped to the E4D mesh before a forward run is executed. In addition to the incongruent alignment of the structured mesh used by PFLOTRAN and the unstructured mesh used by E4D, each mesh will typically differ in scale in different regions of the model domain in order to accurately model the differing physics relevant to subsurface fluid flow and electrical current flow from point sources. For example, the E4D mesh will typically be refined near electrodes to accurately model the large potential gradients near current source electrodes. In these regions the volumes of the elements in the E4D mesh may be much smaller than the PFLOTRAN elements in the same region. Further from the electrodes where the E4D elements become large, the opposite may be true. In order to accommodate both conditions, we integrate the bulk conductivity of the PFLOTRAN mesh over each E4D mesh element. The bulk conductivity is provided at any point in the PFLOTRAN modeling domain using a tri-linear interpolation of the value at the eight PFLOTRAN cell centers surrounding that point. Figure 5 illustrates the general approach. Let m_i^e be the bulk conductivity of element *i* in the E4D mesh. Then

$$m_i^e = \frac{1}{V_i}\int_{V_i} m^c(\mathbf{r})dV \approx \frac{1}{n_k}\sum_{k=1}^{n_k} m_{i,k}^c \qquad \text{eq. 6}$$

where V_i is the volume of E4D mesh element *i*, $\mathbf{r}$ is a position vector, m^c is the bulk conductivity on the PFLOTRAN mesh, n_k is the number of subdivisions by which E4D element *i* is divided for the integral approximation, and $m_{i,k}^c$ is the bulk conductivity within element *i* and subdivision *k*. The value of $m_{i,k}^c$ is determined using a tri-linear interpolation of the values of m^c at each of the eight PFLOTRAN cell centers surrounding point *i,k* ,as illustrated in Figure 5. This gives

$$m_{i,k}^c = \sum_{j=1}^{n_c} m_j^c W_{i,j,k} \qquad \text{eq. 7}$$

where n_c is the number of elements in the PFLOTRAN mesh, m_j^c is the bulk conductivity of element *j* in the PFLOTRAN mesh, and $W_{i,j,k}$ is the weight given to m_j^c in determining the value of sub-element *k* within mesh element *i* of the E4D mesh, determined using the tri-linear interpolation. Note that for a given k, $W_{i,j,k}$ will be zero for all n_c PFLOTRAN elements except for the eight surrounding point *i,k* , resulting in the sparse interpolation matrix shown below.

Combining equations 6 and 7 gives the interpolation equation for an E4D mesh element *i*,

$$m_i^e = \frac{1}{n_k}\sum_{k=1}^{n_k}\sum_{j=1}^{n_c} m_j^c W_{i,j,k} \ . \qquad \text{eq. 8}$$

Equation 8 is expressed in matrix form as

$$\mathbf{m}^e = \mathbf{M}\mathbf{m}^c \qquad \text{eq. 9}$$

where $\mathbf{m}^c$ is an n_c length vector containing the bulk conductivity values on the PFLOTRAN mesh, $\mathbf{m}^e$ is a n_e length vector containing the bulk conductivity values on the E4D mesh, n_e is the number of elements in the E4D mesh, and $\mathbf{M}$ is the $n_e x n_c$ mesh interpolation matrix. Although $\mathbf{M}$ is sparse, its computation is somewhat demanding. However, $\mathbf{M}$ only needs to be computed once, and its computation is highly parallelizable. As shown in figure 1A, $\mathbf{M}$ is computed in parallel by the E4D slave processes during the setup phase. The master node assigns each slave the same number of rows (plus or minus one row) of $\mathbf{M}$ to compute. After each slave computes its assigned rows of $\mathbf{M}$, it returns the results to the master process, which assembles the matrix in a sparse format. As shown in figure 1B, the master process is also responsible for conducting the mesh interpolation multiplication represented by equation 9, and transferring the resulting $\mathbf{m}^e$ vector of bulk conductivity values to the slave processes in preparation for a forward run.

4.8. PFLOTRAN-E4D forward modeling

This section summarizes the forward modeling operations of the PFLOTRAN-E4D module discussed in previous sections. Upon initialization, PFLOTRAN assigns E4D a user specified number of processors. E4D then assigns one processor to be the master process, and the remaining processes as slave processes. The master process reads the E4D input files, passes relevant information to the slave processes, including mesh dimensions and electrode assignments, and instructs the slaves to construct and return the mesh interpolation matrix. The master node then instructs the slaves to build the finite element coupling matrix in preparation to solve equation 1 given the bulk conductivity supplied by PFLOTRAN at each user-specified time step.

At each PFLOTRAN time-step, PFLOTRAN sends E4D the simulated subsurface states necessary to derive bulk conductivity using the petrophysical transform given by equation 5. If user input specifies that an ERT survey should be simulated for the current time step, these states are converted to bulk conductivity and mapped to the E4D mesh by the E4D master node. The E4D master process then broadcasts the bulk conductivity distribution for the current time step to the slave processes, and instructs the slave processes to compute the pole solutions for each electrode assigned. During the pole solution computations, the master process reads a user-specified survey file, indicating which measurements should be extracted from the pole solutions to simulate the ERT survey for the current time step. Upon completion of the pole solutions, the master node broadcasts the measurement sequence to the slave processes. The slave processes then extract the relevant electrode potentials from their respective pole solutions and send them to the master where they are assembled and output to a text file.

5. *Groundwater/Surface water interaction monitoring simulation*

To demonstrate the PFLOTRAN-E4D simulation module, we simulate ERT monitoring of a groundwater/surface-water interaction system along the Columbia River at the Hanford Site 300 Area in south-central WA, USA (Figure 6). Columbia River stage levels at the 300 Area are governed by releases at the Priest Rapids Dam, located approximately 55 km upstream from the study area. Outflows are modulated to manage the competing demands of power generation, flood control, irrigation, and ecological habitat, resulting in dynamic stage variations over a variety of temporal scales. Aquifer sediments bounding the Columbia River are generally coarse grained and highly permeable [*Hammond and Lichtner*, 2010; *Williams et al.*, 2008]. Coupled with dynamic stage variations, the resulting system is characterized by active stage driven intrusion and retreat of river water into the adjacent unconfined aquifer system. During high-stage spring runoff events, river water has been detected in monitoring wells nearly 400 m from the shoreline [*Williams et al.*, 2008].

During baseline, low-stage conditions (October-February), the Columbia River is a gaining stream, and the aquifer pore space is occupied by groundwater. As stage levels rise, two processes induce opposing changes in the bulk electrical conductivity of the aquifer (Johnson et al., 2015b). First, the rising water table causes previously unsaturated sediments to become saturated, resulting in an increase in bulk conductivity near the water table (see equation 5). The second change originates in the contrast between lower conductivity river water, and higher conductivity groundwater. As river stage rises, a hydraulic gradient develops within the aquifer that drives river water inland, displacing higher conductivity groundwater, and decreasing bulk conductivity within the saturated zone.

Computational meshes

Changes in bulk conductivity caused by stage-driven water table fluctuations and river water intrusion were monitored over time in three-dimensions using ERT with a surface array of 352 electrodes during the high stage cycle from April through September of 2013 (Johnson et al., 2015b). In this example we use PLOTRAN with the E4D module to simulate river water intrusion and the corresponding time-lapse ERT surveys over the first 30 days of the experiment. The PFLOTRAN mesh is shown in Figure 7A. Each mesh element is 2m by 2m wide in the horizontal direction, and 0.5 m in the vertical direction, giving 1.6 million elements in total. The mesh is divided into a background host sediment and a higher permeability paleochannel as shown, meant to mimic the paleochannel structures known govern fluid flow in the 300 Area. The E4D mesh is shown in Figure 7B. The mesh was created to conform to the surface topography and riverbed bathymetry as determined from LiDAR data collected over the site. The refined sections of the mesh indicate the locations of electrode lines deployed on the surface. There are 11 lines total with 32 electrodes in each line at 10 m separation. Each line is separated by 25 m. The remainder of the E4D mesh that is not shown in Figure 7B extends 10 km outward in the horizontal directions and downward in the vertical direction, with elements increasing in size with distance from the electrode array. The boundaries are placed far from electrodes to reduce the effects of the zero-potential subsurface boundary conditions used to solve equation 1. In total, the E4D mesh contains 905,185 elements.

To illustrate the alignment between the two meshes, Figure 7C shows the PFLOTRAN mesh superimposed on a transparency of the E4D mesh. Note that the maximum elevation of the water table is 106.7 m, and the PFLOTRAN mesh extends to 110 m to enable simulation of stage-driven changes in saturation and pore water conductivity in both the saturated and unsaturated zones. It is not necessary for the PFLOTRAN mesh to extend to the surface, so it is effectively embedded within the E4D mesh. PFLOTRAN elements located above the river channel (figure 7C) are inactive in the simulation, such that the PFLOTRAN mesh conforms to the river bathymetry (not shown).

Material Properties

The hydrogeologic properties of the host material and paleochannel used for the PFLOTRAN simulation are shown in table 1 below. The unsaturated hydraulic conductivity is computed using the Van Genuchten water retention function [*Vangenuchten*, 1980] and the Burdine permeability relationship [*Burdine*, 1953].

Table 1. Hydrogeologic material properties of host material and channel shown in Figure 7.

Material	**Porosity**	**Permeability (m^2)**	**Van Genuchten/Burdine Parameters**		
			Res. Sat.	m	alpha
Host	0.30	1.05e-9	0.13	0.748	1.43E-4
Channel	0.20	4.39e-9	0.16	0.340	7.27E-4

Boundary and Initial Conditions

Both pressure and solute concentration boundary and initial conditions are required for the PFLOTRAN simulation. At the northern, western, and southern boundaries of the PFLOTRAN mesh, transient (hydrostatic) head conditions were applied using kriging-based interpolations of hourly water table elevation measurements in wells inside and beyond the model domain, an approach similar to the one described in detail by Chen et al. (2013). At the eastern boundary (i.e. the river bed boundary), transient head boundary conditions are described using river stage measured by a pressure transducer deployed close to the southeastern edge of our model domain (Figure 8), and the gradient along the river was estimated using water elevation data in a network of wells located close to river shoreline. A conductance value of 10^{-12} m was applied to the eastern boundary to mimic the damping effect of low-permeability material on the river bed, which was adopted from an earlier simulation study at the Hanford Site (Williams et al., 2008, Hammond et al., 2010). A no-flow boundary condition was specified at the bottom of the domain since the domain is underlain by low permeability Ringold Formation materials, and a small constant-rate recharge boundary condition of 55 mm/yr was applied at the top of the model domain.

River water intrusion was tracked by introducing a conservative tracer at the river boundary. The concentration boundary conditions for the tracer were set to be free outflow at the northern, western, and southern boundaries, while a constant concentration was maintained at the river boundary. The recharge water at the upper boundary was set to be tracer free, while a zero-flux tracer boundary condition was applied at the lower now flow boundary.

The initial flow condition was a hydrostatic pressure distribution based on the water table, as interpolated from the same set of wells that were used to create the transient lateral flow boundary conditions at the northern, western, and southern boundaries. The initial conservative tracer concentration was set to be zero over the entire model domain.

As previously described, zero potential boundary conditions are specified on the subsurface boundaries of the E4D mesh, which are located far from the electrode array. Zero current flux boundary conditions are specified normal to the surface boundary. There are many E4D elements that are not within the PFLOTRAN modeling domain, and are therefore not influenced by the PFLOTRAN simulation. Those elements assume a user specified bulk conductivity provided at each time step through input files, which is in this case the bulk conductivity provided by the equation 5 at time zero given the material properties specified in table 1.

Petrophysical Transformation

We assume for the simulation that each variable in equation 5 is known and constant through time, except for fluid conductivity and saturation, which are simulated by PFLOTRAN given the material properties listed in table 1 and boundaries conditions described in the previous section. PFLOTRAN simulates river water as a conservative tracer, and provides the river water fraction to E4D at each time step. E4D converts river water fraction to fluid conductivity using a linear interpolation between the end members of groundwater fluid conductivity (0.040 S/m) and river water fluid conductivity (0.015 S/m) as determined from direct field measurements. The resulting fluid conductivity distribution and saturation provided by PFLOTRAN are used with equation 5 to compute bulk conductivity, which is then interpolated to the E4D mesh and sent to the E4D slave nodes for forward computations.

6. Results

The simulation previously described was executed using 481 compute cores on a distributed memory parallel computing machine. In total, 128 cores were allocated to PFLOTRAN and 353 cores were allocated to the E4D module (1 master and 352 slaves, one for each electrode). With this allocation, E4D was able to complete a forward simulation (from mesh interpolation through output) within the time required for a single PFLOTRAN time-step, so there was no additional computation time required beyond that required for PFLOTRAN alone. The entire simulation required approximately 3 hours for completion on the Olympus supercomputer housed at the Pacific Northwest National Laboratory (http://pic.pnnl.gov/resources.stm).

Given the high permeability of sediments in the simulation, the groundwater table is at all times near the river stage elevation. With this in mind, we demonstrate the results of the PFLOTRAN simulation, petrophysical transformation, and mesh interpolation at two times (5 days and 15 days) and at two elevations, one below the water table (105 m), and one above the water table (107 m). At 5 and 15 days the river stage is at approximately 105.8 m and 106.4 m respectively (Figure 8). Figure 9 shows the change in saturation and river water fraction from baseline conditions at 105 m and 107 m simulated by PFLOTRAN, and on the PFLOTRAN mesh (upper panels). The lower panels show the corresponding changes in bulk conductivity derived from the petrophysical transform, interpolated onto to the E4D mesh.

The performance of the mesh interpolation scheme is evident by comparing the change in river water fraction (PFLOTRAN mesh) to the change in bulk conductivity (E4D mesh) at 105 m for each time shown. Since the subsurface is fully saturated at 105 m, the relationship between a change in fluid conductivity and a change in bulk conductivity is linear, meaning the spatial distribution of the changes should be identical at this elevation. The 105 m images in Figure 9 show this to be the case, and demonstrate the performance of the mesh interpolation scheme. The same images show the expected behavior of river water intrusion to flow preferentially into the high permeability paleochannel, and the corresponding decrease in bulk conductivity as river water replaces groundwater in the pore space. The uneven river water/groundwater front within the host material (i.e. outside of the channel) is caused by variability in the river bottom bathymetry incorporated into the PFLOTRAN mesh.

The effects of the differing material properties shown in table 1 are highlighted by the change in saturation plots at the 107 m elevation. At both 5 and 15 days, saturation at 107 m increases within the host material as the water table rises, but saturation increase within the channel is relatively minor. The river water fraction plots show that pore water moving upward into the unsaturated zone is primarily groundwater at 5 days, suggesting the corresponding change in bulk conductivity at 5 days and 107 m elevation is caused primarily by an increase in saturation with groundwater. Conversely, the change in conductivity at 15 days and 107 m elevation bares the imprint of the river water intrusion within the saturated zone. The conductivity increase within the vadose zone above the river water intrusion zone is subdued as lower conductivity river water moves into the unsaturated zone through capillary action. Overall, the simulation demonstrates the complex nature of stage driven changes in bulk conductivity associated with this relatively simple synthetic representation of the 300 Area, including complex patterns of conductivity increase within the vadose zone, underlain by decreases in conductivity within the saturated, river water intrusion zone.

Figure 10 shows the E4D-simulated change in electrical potential on the surface from conditions at time zero, and for three different current injection points. The current electrodes for each of the three measurement configurations (M1, M2, and M3) are arranged in a Wenner Alpha array, whereby the two potential measurement electrodes are placed in between the current electrodes, with equal spacing between any two adjacent electrodes. In each case that spacing is 20m. The locations of each measurement are shown in Figure 10A. M1 is located near the shoreline directly over the paleochannel. M2 is located outside of paleochannel and near the shoreline. M3 is located within the paleochannel, far from the shoreline. For each measurement, the positive current electrode is to the south, the negative current electrode is to the north. Figure 10B shows the change in potential on the ground surface for each measurement, normalized to 1 ampere of injected current, at 5 and 15 days. At 5 days measurements M2 and M3 show similar patterns of potential difference that are caused primarily by the rising water table, because M2 and M3 do not overlie the river water intrusion zone at 5 days (see Figure 9). Contrast this to M1, which does overlie the intrusion zone at 5 days, and displays a significantly different potential difference pattern compared to M2 and M3. At 15 days, the potential difference distributions for all measurements have changed significantly compared to 5 days. This demonstrates the sensitivity of the ERT measurements to stage driven hydrodynamics, and verifies the corresponding opportunity to image stage-driven changes in electrical conductivity using time-lapse ERT.

To further illustrate this point, Figure 11 shows the time series for the potentials measured at M1, M2, and M3 superimposed on the river stage elevation shown in figure 8. Note that the simulated potentials are normalized by the injected current to give the transfer resistance. If the support volume for a given measurement becomes less conductive (more resistive), then the transfer resistance will increase, and vice versa. The transfer resistance time series are informative in this regard. M1 displays and increasing trend in transfer resistance, indicating that the subsurface within the support volume for M1 is becoming more resistive, on average. This is consistent with the location of M1, directly over the channel and near the shoreline, where the measurement support volume is primarily influenced by more resistive river water. Note however the influences of water table variations are not lost on the same time series. When river stage (and thus water table) drop, the M1 time series displays a corresponding increase in transfer resistance correspond to the decrease in saturation associated with the falling water table, and vice versa. The same can be observed for M2 and M3. Measurements M2 and M3 are primarily influenced by the river stage-driven increase in water table elevation up to about day 10. The rising water table causes an increase in saturation and corresponding decrease in resistivity, as evidenced by the decreasing transfer resistance over that period. After day 10 the transfer resistance begins to increase in M2 and M2 as more resistive river water begins to enter support volume of each measurement.

7. Discussion

In the introduction we stated that a multi-physics simulator capable of modeling the bulk electrical conductivity evolution arising from a given subsurface processes would, among other things, 1) enable practitioners to investigate the feasibility of monitoring that process using ERT, and 2) enable the discovery of critical electrical signatures associated with the process, and the exploitation of that signature for effective process monitoring. The groundwater/surface water interaction simulation presented in sections 5 and 6 is illustrative in this regard. First, the simulation demonstrated that contrasts in bulk conductivity originating from stage-driven river water intrusion provide ERT measurements with adequate sensitivity for monitoring (Figure 11), thereby demonstrating the feasibility of 4D ERT monitoring of river water intrusion and retreat. Second, the simulation revealed the contrasting influences of water table fluctuations and river water intrusion on the bulk conductivity distribution along with the relative magnitudes of those influences in terms of the corresponding ERT measurements (Figure 11). In terms of electrical signatures, those measurements that are not influenced by river water intrusion are characterized by a decrease in transfer resistance with respect to baseline conditions associated with the rising water table. Only measurements that are influenced by river water intrusion experience an increase in transfer resistance compared to baseline conduction. As shown by Wallin et al. (2013) and Johnson et al. (2015b), the ERT data alone do not provide sufficient information to resolve between these competing influences using standard ERT inversion algorithms. Recognition of this fact enabled the development of customized constraints that allowed only increase in bulk conductivity within the vadose zone, and decreases in conductivity within the saturated zone, in relation to baseline conditions (Figure 9). These constraints provided the imaging algorithm with the information necessary to delineate between the influences of water table fluctuations and river water intrusion, thereby enabling effective imaging of the river water intrusion zone. We expect the coupled PFLOTRAN-E4D modeling demonstrated here will provide similar utility in other ERT monitoring applications of complex systems.

It is well recognized that geophysical data, particularly time lapse geophysical data, have the potential to significantly reduce uncertainty in hydrogeologic parameter estimations [*Dafflon et al.*, 2011; *Jardani et al.*, 2013; *Linde et al.*, 2006; *Pollock and Cirpka*, 2012]. Progress toward information hydrogeologic inversions with geophysical data is complicated by the general requirement for an accurate field scale petrophysical transform, and by the computational demands of simulating both the hydrological and geophysical observations. The latter can be addressed in part through high performance computing and suitable codes such as PFLOTRAN-E4D. We also note the many advantages of the open source license provided by PFLOTRAN-E4D, which facilitates transparency and collaboration, and enables users to modify the code as needed for custom applications.

8. Acknowledgements

This research was supported by the U.S. Department of Energy (DOE), Office of Biological and Environmental Research (BER), as part of BER's Subsurface Biogeochemistry Research Program (SBR). This contribution originates from the SBR Scientific Focus Area (SFA) at the Pacific Northwest National Laboratory (PNNL).

9. References

Archie, G. E. (1942), The electrical resistivity log as an aid in determining some reservoir characteristics, T Am I Min Met Eng, 146, 54-61.

Balay, S., J. Brown, K. Buschelman, V. Eijkhout, W. D. Gropp, D. Kaushik, M. G. Knepley, L. C. McInnes, B. F. Smith, and H. Zhang (2015), PETSc Users Manual, Tech. Rep. ANL-95/11—Revision 3.5, Argonne Natl. Lab., Argonne, Ill.

Binley, A., S. S. Hubbard, J. A. Huisman, A. Revil, D. A. Robinson, K. Singha, and L. D. Slater (2015), The emergence of hydrogeophysics for improved understanding of subsurface processes over multiple scales, Water Resour Res, 51(6), 3837-3866.

Burdine, N. T. (1953), Relative Permeability Calculations from Pore Size Distribution Data, T Am I Min Met Eng, 198, 71-78.

Chen, X., G. E. Hammond, C. J. Murray, M. L. Rockhold, V. R. Vermeul, and J. M. Zachara (2013), Application of ensemble-based data assimilation techniques for aquifer characterization using tracer data at Hanford 300 area, Water Resour Res, 49(10), 7064-7076.

Daily, W., and E. Owen (1991), Cross-Borehole Resistivity Tomography, Geophysics, 56(8), 1228-1235.

Gropp, W., E. Lusk, and R. Thakur (1999), Using MPI-2: Advanced Features of the Message-Passing Interface, MIT Press.

Hammond, G. E., and P. C. Lichtner (2010), Field-scale model for the natural attenuation of uranium at the Hanford 300 Area using high-performance computing, Water Resour Res, 46.

Hammond, G. E., P. C. Lichtner, and R. T. Mills (2014), Evaluating the performance of parallel subsurface simulators: An illustrative example with PFLOTRAN, Water Resour Res, 50(1), 208-228.

Johnson, T. C., and D. M. Wellman (2015), Accurate modelling and inversion of electrical resistivity data in the presence of metallic infrastructure with known location and dimension, Geophys. J. Int., 202(2), 1096-1108.

Johnson, T., R. Versteeg, J. Thomle,G. Hammond, X. Chen, and J. Zachara(2015b), Four-dimensional electricalconductivity monitoring ofstage-driven river water intrusion:Accounting for water table effectsusing a transient mesh boundary andconditional inversion constraints,Water Resour. Res., 51, 6177–6196,doi:10.1002/2014WR016129.

Johnson, T. C., R. J. Versteeg, A. Ward, F. D. Day-Lewis, and A. Revil (2010), Improved hydrogeophysical characterization and monitoring through parallel modeling and inversion of time-domain resistivity and induced-polarization data, Geophysics, 75(4), Wa27-Wa41.

Lichtner, P.C., G.E. Hammond, C. Lu, S. Karra, G. Bisht, B. Andre, R.T. Mills and J. Kumar (2015) PFLOTRAN Users Manual, www.pflotran.org.

Kemna, A., A. Binley, F. Day-Lewis, A. Englert, B. Tezkan, J. Vanderborght, H. Vereecken, and P. Winship (2006), Solute transport processes, Nato Sci S Ss Iv Ear, 71, 117-159.

Revil, A. (2013), Effective conductivity and permittivity of unsaturated porous materials in the frequency range 1 mHz-1GHz, Water Resour Res, 49(1), 306-327.

Revil, A., M. Karaoulis, T. Johnson, and A. Kemna (2012), Review: Some low-frequency electrical methods for subsurface characterization and monitoring in hydrogeology, Hydrogeol J, 20(4), 617-658.

Rucker, C., T. Gunther, and K. Spitzer (2006), Three-dimensional modelling and inversion of dc resistivity data incorporating topography - I. Modelling, Geophys J Int, 166(2), 495-505.

Singha, K., F. D. Day-Lewis, T. Johnson, and L. D. Slater (2015), Advances in interpretation of subsurface processes with time-lapse electrical imaging, Hydrol Process, 29(6), 1549-1576.

Slater, L. (2007), Near surface electrical characterization of hydraulic conductivity: From petrophysical properties to aquifer geometries - A review, Surv Geophys, 28(2-3), 169-197.

Vangenuchten, M. T. (1980), A Closed-Form Equation for Predicting the Hydraulic Conductivity of Unsaturated Soils, Soil Sci Soc Am J, 44(5), 892-898.

Williams, M. D., M. L. Rockhold, P. D. Thorne, and Y. Chen (2008), Three-Dimensional Groundwater Models of the 300 Area at the Hanford Site, Washington StateRep., Pacific Northwest National Laboratory, Richland, WA.

Commer, M., M. B. Kowalsky, J. Doetsch, G. A. Newman, and S. Finsterle (2014), MPiTOUGH2: A parallel parameter estimation framework for hydrological and hydrogeophysical applications, Comput Geosci-Uk, 65, 127-135.

Dafflon, B., W. Barrash, M. Cardiff, and T. C. Johnson (2011), Hydrological parameter estimations from a conservative tracer test with variable-density effects at the Boise Hydrogeophysical Research Site, Water Resour Res, 47.

Jardani, A., A. Revil, and J. P. Dupont (2013), Stochastic joint inversion of hydrogeophysical data for salt tracer test monitoring and hydraulic conductivity imaging, Adv Water Resour, 52, 62-77.

Linde, N., J. S. Chen, M. B. Kowalsky, and S. Hubbard (2006), Hydrogeophysical parameter estimation approaches for field scale characterization, Nato Sci S Ss Iv Ear, 71, 9-44.

Pollock, D., and O. A. Cirpka (2012), Fully coupled hydrogeophysical inversion of a laboratory salt tracer experiment monitored by electrical resistivity tomography, Water Resour Res, 48.

Rings, J., J. A. Huisman, and H. Vereecken (2010), Coupled hydrogeophysical parameter estimation using a sequential Bayesian approach, Hydrol Earth Syst Sc, 14(3), 545-556.

Figures

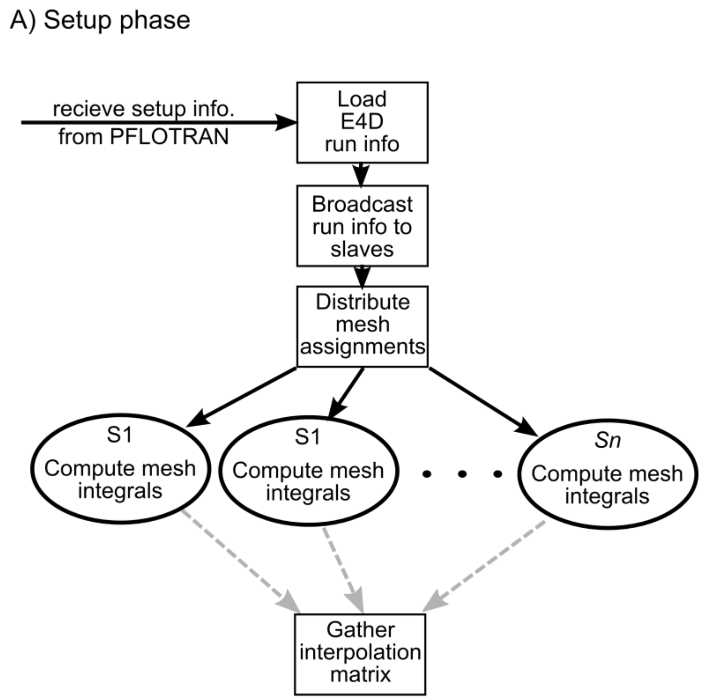

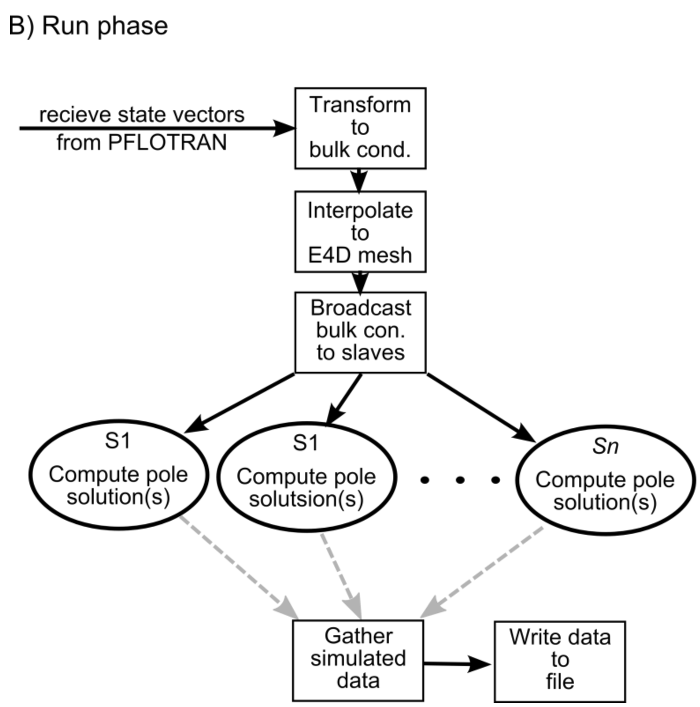

Figure 1. Flow diagram showing the setup and run phases of the E4D module. A) In the setup phase, E4D is initialized by PFLOTRAN. The master node receives setup and instructs the slave nodes to construct the PFLOTRAN-E4D mesh interpolation matrix. B) At each time step, the E4D master node

receives subsurface state information from PFLOTRAN, converts that information to bulk conductivity with a user supplied petrophysical transform, maps the bulk conductivity to the E4D mesh, and transfers the results to the slave nodes. The slave nodes compute pole solutions for assigned electrodes, and transfer the relevant potentials to the master node for assembly. The master node assembles the potentials to create the simulated measurements, and writes the results to a file.

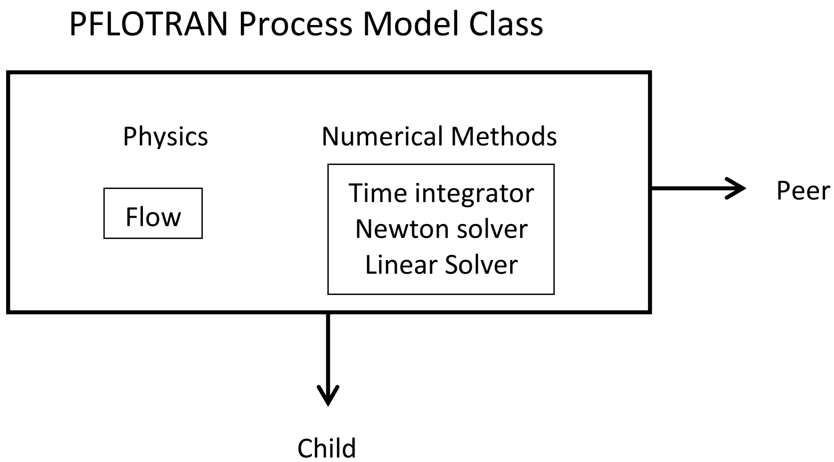

Figure 2. The PFLOTRAN process model class coupling physics/chemistry to numerical methods for their solution. Each process model has a pointer to a neighboring peer and child, which enables linkage between process models through a tree data structure (tree graph theory).

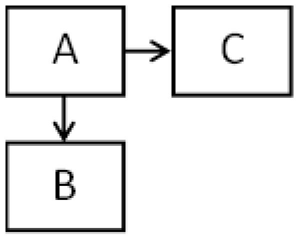

Figure 3. Example process model tree with master process model A linked to child B and peer C. Process model B follows A’s time stepping (either lock step or through sub-steps) while A and C synchronized at specified points in time.

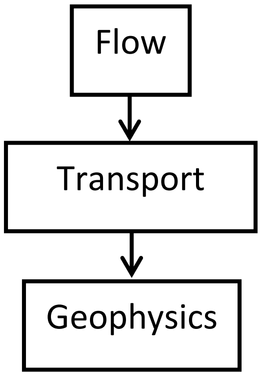

Figure 4. The process model tree for PFLOTRAN-E4D coupling where single-phase variably saturated flow is the master process model with solute transport as its child and geophysics is the child of transport. In most cases, all three process models proceed lock step with each other (flow → transport → geophysics).

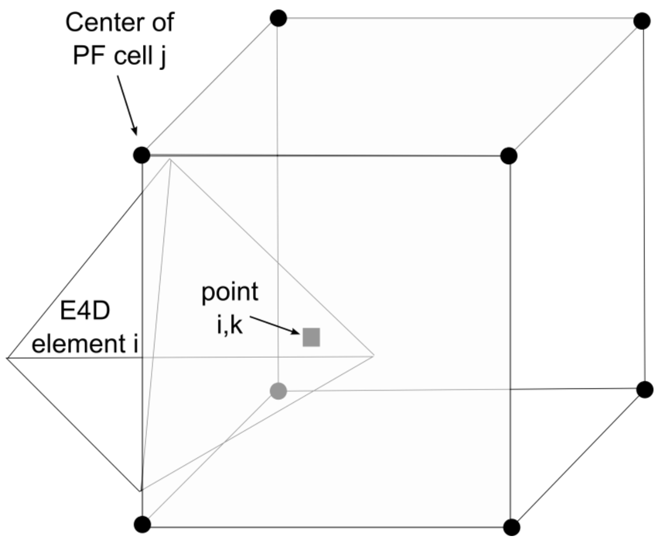

Figure 5. Components used to interpolate bulk conductivity from the PFLOTRAN mesh to the E4D mesh.

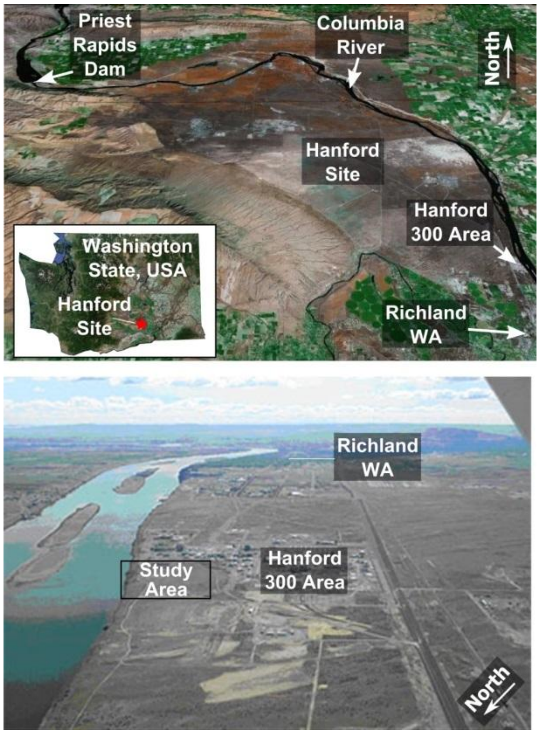

Figure 6. Location of simulated study area along the Columbia River at the Hanford 300 Area in south-central WA, USA.

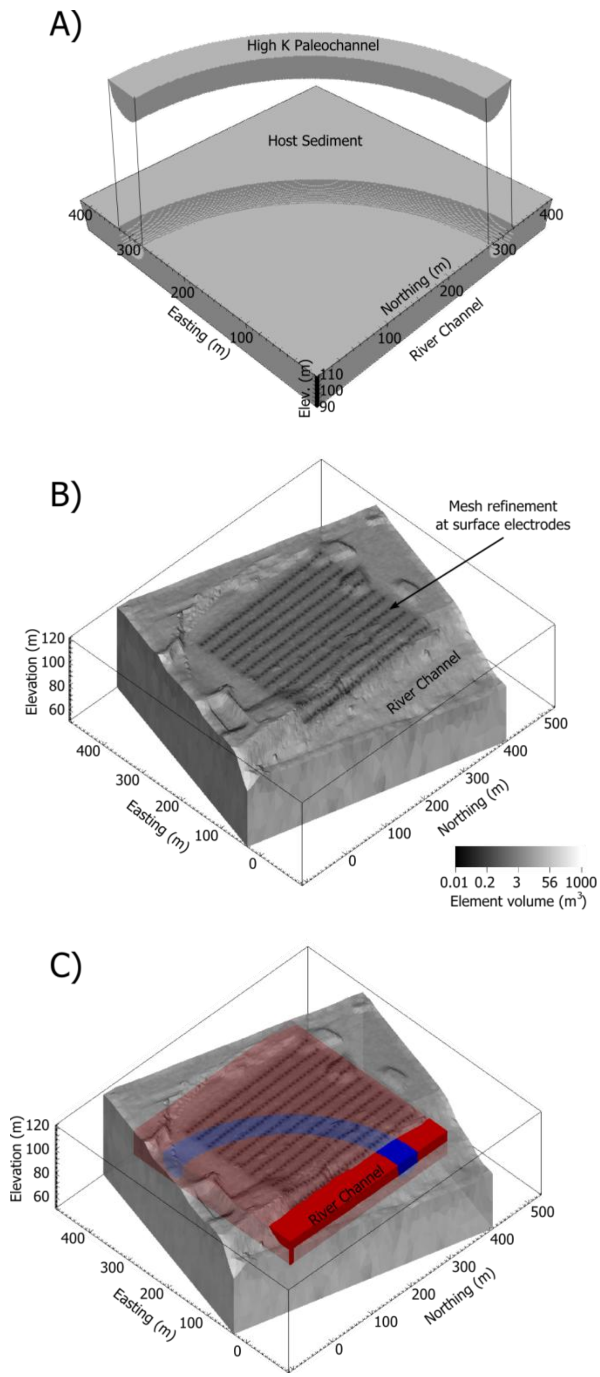

Figure 7. A) PFLOTRAN computational mesh showing high permeability paleochannel embedded in a lower permeability host sediment. B) Interior E4D mesh showing surface topography and mesh refinement at electrode locations. C) PFLOTRAN mesh (blue channel and red host material) superimposed on a transparent view of the E4D mesh.

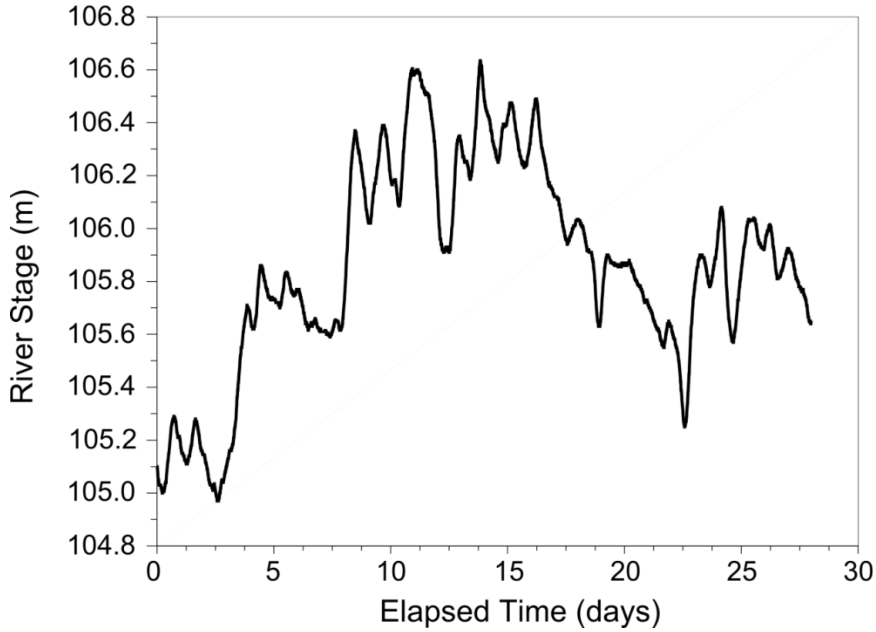

Figure 8. River stage during simulation period (April 1 – April 28, 2013).

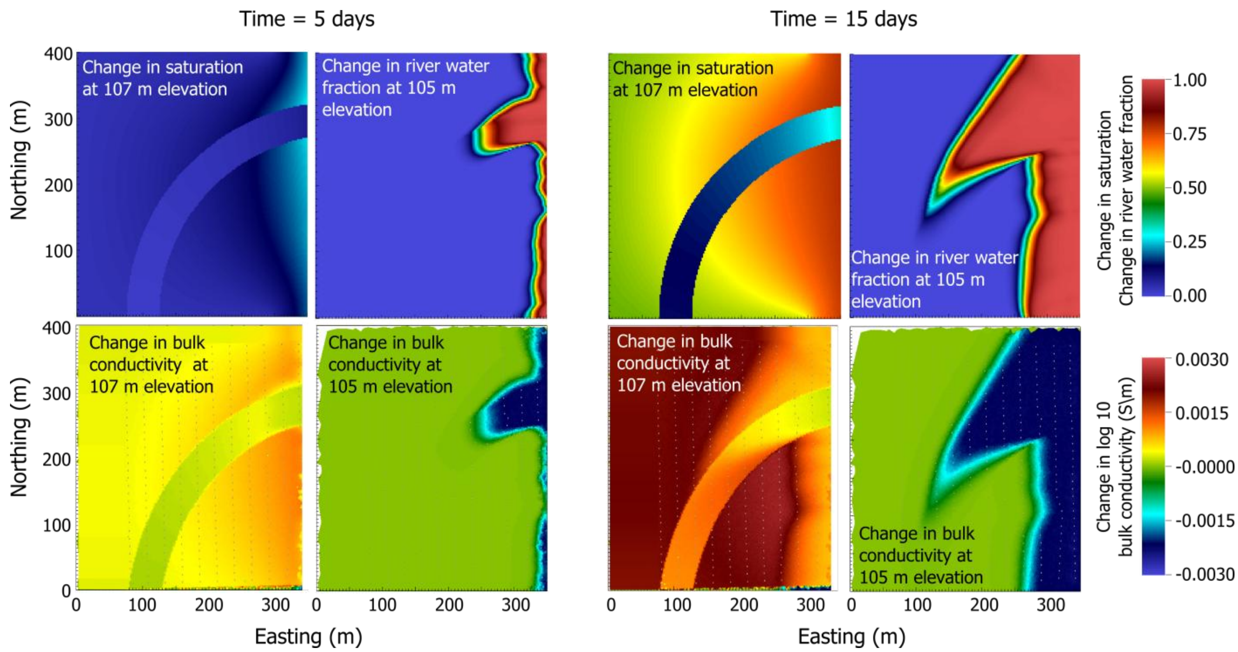

Figure 9. (Top Row) Simulated change in saturation and river water fraction from baseline conditions on the PFLOTRAN mesh at 5 and 15 days, and at 105 m and 107 m elevation. (Bottom Row) Simulated change in bulk electrical conductivity from baseline conditions at 5 and 15 days, and at 105 m and 107 m elevation.

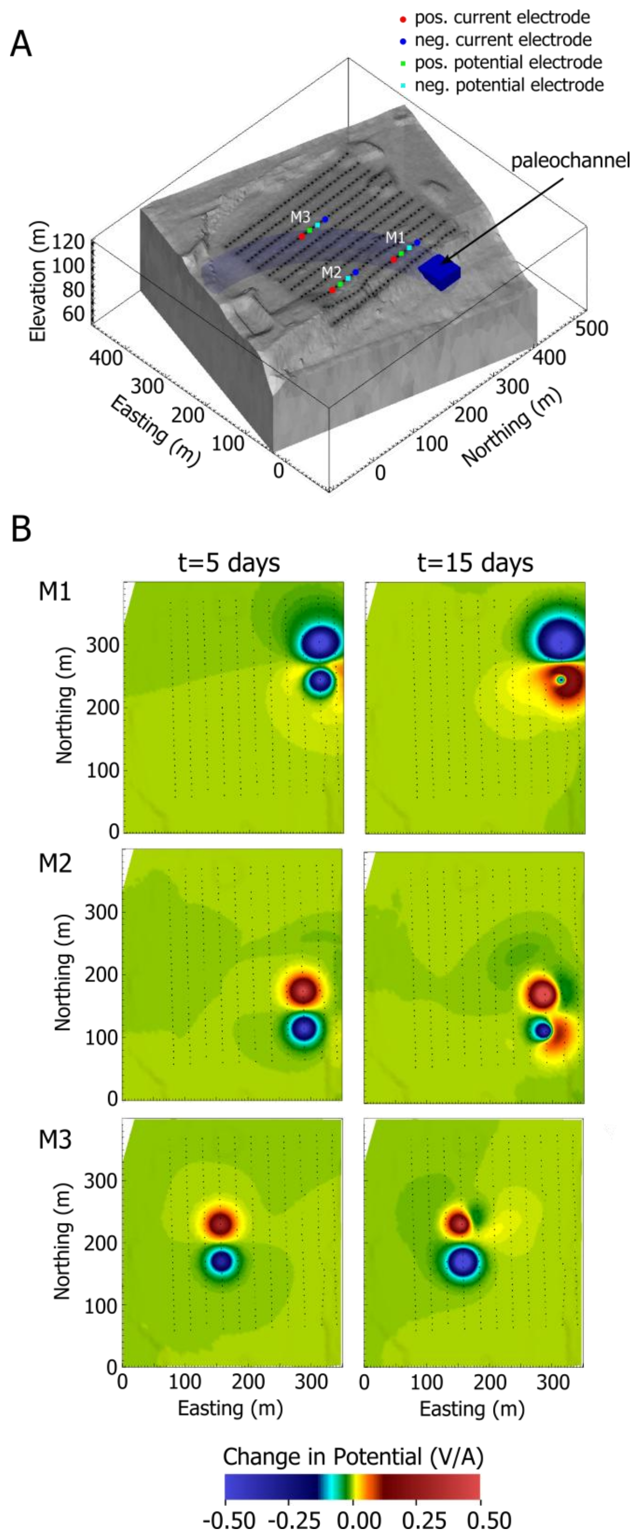

A
pos. current electrode
neg. current electrode
pos. potential electrode
neg. potential electrode
paleochannel
M3
M1
M2
Elevation (m)
120
100
80
60
400
300
200
100
0
Easting (m)
0
100
200
300
400
500
Northing (m)
B
t=5 days
t=15 days
M1
M2
M3
Northing (m)
0
100
200
300
Easting (m)
0
100
200
300
Change in Potential (V/A)
-0.50
-0.25
0.00
0.25
0.50

Figure 10. A) Locations of the three (M1-M3) 4-electrode Wenner measurements demonstrated in (B) and in figure 8. B) Change in surface potential per ampere of current injected for measurements M1-M3, at 5 and 15 days.

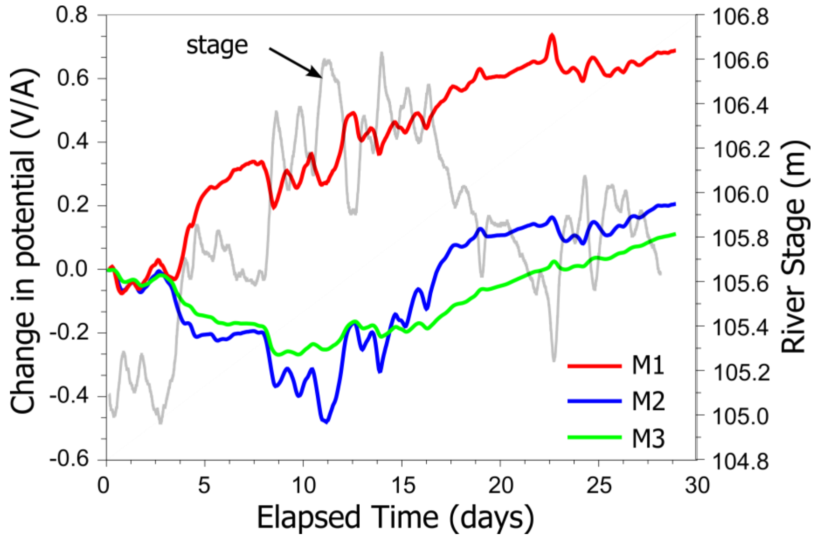

Figure 11. Transfer resistance time series for measurements M1-M2 (see figure 7) superimposed on the river stage elevation.